



Chaos and the limits of predictability for the solar-wind-driven magnetosphere–ionosphere system

W. Horton, R. S. Weigel, and J. C. Sprott

Citation: [Physics of Plasmas \(1994-present\)](#) **8**, 2946 (2001); doi: 10.1063/1.1371522

View online: <http://dx.doi.org/10.1063/1.1371522>

View Table of Contents: <http://scitation.aip.org/content/aip/journal/pop/8/6?ver=pdfcov>

Published by the [AIP Publishing](#)

Articles you may be interested in

[Role of the solar wind in the structure and dynamics of magnetospheres](#)

AIP Conf. Proc. **1539**, 376 (2013); 10.1063/1.4811064

[Ionospheric Response to the Interplanetary Shock](#)

AIP Conf. Proc. **974**, 52 (2008); 10.1063/1.2885033

[Electrodynamics of the magnetosphere–ionosphere coupling in the nightside subauroral zone](#)

Phys. Plasmas **11**, 1260 (2004); 10.1063/1.1647139

[Geomagnetic transport in the solar wind driven nightside magnetosphere–ionosphere system](#)

Phys. Plasmas **9**, 3712 (2002); 10.1063/1.1499119

[The solar-wind driven magnetosphere–ionosphere as a complex dynamical system](#)

Phys. Plasmas **6**, 4178 (1999); 10.1063/1.873683



Chaos and the limits of predictability for the solar-wind-driven magnetosphere–ionosphere system

W. Horton and R. S. Weigel

Department of Physics and Institute for Fusion Studies, The University of Texas, Austin, Texas 78712

J. C. Sprott

Department of Physics, University of Wisconsin, Madison, Wisconsin 53706

(Received 2 August 2000; accepted 20 March 2001)

The solar-wind-driven magnetosphere–ionosphere exhibits a variety of dynamical states including low-level steady plasma convection, episodic releases of geotail stored plasma energy into the ionospheric known broadly as substorms, and states of continuous strong unloading. The WINDMI model [J. P. Smith *et al.*, *J. Geophys. Res.* **105**, 12 983 (2000)] is a six-dimensional substorm model that uses a set of ordinary differential equations to describe the energy flow through the solar wind–magnetosphere–ionosphere system. This model has six major energy components, with conservation of energy and charge described by the coupling coefficients. The six-dimensional model is investigated by introducing reductions to derive a new minimal three-dimensional model for deterministic chaos. The reduced model is of the class of chaotic equations studied earlier [J. C. Sprott, *Am. J. Phys.* **68**, 758 (2000)]. The bifurcation diagram remains similar, and the limited prediction time, which is in the range of three to five hours, occurs in the chaotic regime for both models. Determining all three Lyapunov exponents for the three-dimensional model allows one to determine the dimension of the chaotic attractor for the system. © 2001 American Institute of Physics. [DOI: 10.1063/1.1371522]

I. INTRODUCTION

The solar-wind-driven magnetosphere–ionosphere is a complex driven–damped dynamical system. The system exhibits a variety of dynamical states that include low-level steady plasma convection, episodic (quasiperiodic) releases of geotail stored plasma energy into the ionosphere known broadly as substorms, and states of continuous strong unloading provisionally identified as magnetic storms. As in tropospheric weather modeling the lack of predictability can arise from (i) errors in the initial values of the input data, (ii) chaotic fluctuations in the forcing functions, and (iii) internal chaotic dynamics from nonlinearity and feedback loops in the deterministic system. Separating the internal chaos from the externally driven chaos is a well-known difficult problem addressed in Ref. 1. In a recent work,² we analyze the effect of a chaotic solar wind input signal of known fractal dimension on the internal deterministic chaos of a simple model for the nonlinear convection in the magnetosphere (namely, the three-dimensional Lorenz system of equations).

Here, in the present work, we take the solar wind as regular and typically constant, and we ask about the nature of the internal deterministic chaos due to the lack of predictability. The model used for the magnetosphere is the WINDMI model, which is a well-accepted mathematical-physics model for the solar-wind-driven magnetospheric–ionospheric system. The properties of the WINDMI model have been developed in earlier works, with the most recent being Smith *et al.*³ concerning the bifurcation sequences in the system. The physics of the model and its relation with earlier models is given in the review papers of Klimas *et al.*⁴ and Baker *et al.*⁵ Here we examine the lack of predictability that is

intrinsic to this model for a certain range of the system parameters. Other ranges of parameters may show different details in the behavior but are thought to be similar in nature to those used here. For more details on the full range of dynamical behavior see Ref. 3.

In Sec. II we describe the WINDMI model. In Sec. III we give the WINDMI state S3 and briefly discuss the bifurcation properties of the system comparing the physics model with nonlinear filter models. In Sec. IV we derive the reduced three-dimensional (3-D) system and give its properties. In Sec. V we compare some properties of the full and reduced systems, and in Sec. VI we present our conclusions.

II. THE WINDMI SUBSTORM MODEL

The considerable variety of observational forms in the substorm category of events suggests that the appropriate behavior is that of a chaotic system. Within this complex variety of temporal wave forms there is a global spatial coherence described in Ref. 5 that suggests that the appropriate behavior may be that of a low-dimensional dynamical system. Vassiliadis *et al.*⁶ analyzed the auroral AE time series and concluded that the signal is consistent with a low-dimensional chaotic system.

Briefly stated, the global spatial coherence emphasized by Ref. 5 is found in the correlated measurements from (1) the ground-based auroral latitude chain of magnetometers whose wave forms are used to give the classic definition of a substorm event; and (2) the satellite measurements of particle distributions and electromagnetic fields in the geotail plasma containing the large cross-tail current loop $I(t)$ that provides confinement of the high-mean plasma pressure $p(t)$

plasma. High pressure here means that the volume-averaged plasma pressure $\langle p \rangle$ is comparable to the lobe field magnetic pressure $B_l^2/2\mu_0$ produced by the large ($\geq 2 \times 10^7$ A) geotail current loop. The solar wind voltage V_{sw} driving the system arises from the solar wind–Earth magnetic dipole dynamo electric field that maps into the geotail plasmas as the potential $V(t)$ producing the $\mathbf{E} \times \mathbf{B}$ plasma convection. Satellites measure large parallel plasma ion flow velocities, which are described by the energy variable $K(t)$. The final pair of dynamical variables are the parallel field-aligned plasma current, $I_1(t)$, also inferred by satellites from $\delta \mathbf{B}_\perp$, and the ionospheric-voltage imprint $V_i(t)$ of the geotail voltage $V(t)$ onto the ionosphere. The physics of the model is given in Refs. 7 and 8, where diagrams of the somewhat complicated three-dimensional magnetospheric–ionospheric geometry are given. The model is called WINDMI for the solar-wind-driven magnetosphere–ionosphere coupled systems.

The WINDMI model is a six-dimensional (6-D) physics model that describes quantitatively the distribution of the energy flux through the system, through a set of ordinary differential equations derived from basic plasma physics properties of the system. There are six major energy components of the system, with the conservation of energy and charge described by the coupling coefficients in the nonlinear system of differential equations. A variational derivation of the WINDMI model is given in Ref. 8, and the mathematical properties of the states described by the WINDMI model are given in Ref. 3. Here we focus on the system described as S3 in Smith *et al.*:³ a state that characterizes many features of the substorm dynamics as the solar wind dynamo voltage, V_{sw} , increases from low to high values.

We will investigate two questions concerning the WINDMI description of the substorm dynamics. First, we ask whether the six-dimensional energy system can be reduced to the minimal order three-dimensional system of a deterministic chaotic system described by ordinary differential equations. In particular, we also examine what is lost by this series of reductions. In making the reduction to a three-dimensional system, the faster-evolving energy components are taken analytically to be given by their local fixed point or “equilibrium” values. In making this replacement, the energy and charge conserving features of the full ODE system are lost during rapid transients. The only practical method of judging how much fidelity is lost by these reductions is by comparing the dynamics of the full and reduced system. While there are differences in the solutions, we show that the minimal three-dimensional system dynamics parallels that of the full system in many ways.

Second, we ask what the minimal model tells us about the intrinsic limits of predictability in the system. In the process of making the reduction to the three-dimensional system we isolate the essential nonlinearity in the system. We show that the unloading function in the pressure equation is the intrinsic origin of the chaotic dynamics. The other nonlinearities, such as that of the increasing ionosphere conductivity with the increasing power deposited through the ionospheric current system, modify the dynamics in ways consistent with the changes described by Ref. 9. While important, this ionospheric nonlinearity is not the origin of the

complex series of bifurcations and inverse bifurcations contained in the WINDMI model.

A valuable property of low-order dynamical models is the relative precision with which the Lyapunov exponents for the tangent flows can be calculated.¹⁰ The largest Lyapunov exponent, designated as LE, determines the rate of divergence of neighboring trajectories. For a positive LE the reciprocal is then for one e -folding of neighboring orbits and sets the limit of predictability. For typical solar wind conditions we will show that the intrinsic time limit is of order three hours for moderately strong solar wind driving voltages.

Determining all three Lyapunov exponents for the minimal model also allows us to determine the Lyapunov dimension¹¹ of the chaotic attractor for the system as $D_L \cong 2.12$. We compare this result with that calculated from the correlation dimension of 2.14 and with that given earlier for a very simple analog model made up of a Rössler chaotic solar wind driving a Lorenz magnetosphere–ionosphere model system in Refs. 12 and 13.

A benchmark for modeling the nearly constant solar wind input voltage is the 30 h long passage of a magnetic cloud event on January 14/15, 1988 in which a coherent, slowly rotating, large (10–20 nT) interplanetary magnetic field (IMF) passed over the Earth. The Farrugia *et al.*¹⁴ synopsis of the magnetosphere–ionosphere activity during this event showed that 22 substorms occurred during the 18 h period of $B_z(\text{IMF}) < 0$ during which V_{sw} is substantial. This magnetic cloud event was modeled in Ref. 13, where the lobe inductance was calculated as a function of the IMF magnetic field. The baseline values of the physics parameter vector \mathbf{P} were calculated in Refs. 7, 8 with the use of standard magnetospheric physics models.

III. THE WINDMI STATE S3

The WINDMI dynamical model of the Earth’s magnetosphere is a set of six first-order ordinary differential equations whose solutions are chaotic for values of the parameter vector \mathbf{P} of interest. Smith *et al.*³ expressed these equations in dimensionless form as

$$\frac{dI}{dt} = a_1(V_{sw} - V) + a_2(V - V_i), \quad (1)$$

$$\frac{dV}{dt} = b_1(I - I_1) - b_2 P^{1/2} - b_3 V, \quad (2)$$

$$\frac{dP}{dt} = V^2 - K_\parallel^{1/2} P \{1 + \tanh[d_1(I - 1)]\}/2, \quad (3)$$

$$\frac{dK_\parallel}{dt} = P^{1/2} V - K_\parallel, \quad (4)$$

$$\frac{dI_1}{dt} = a_2(V_{sw} - V) + f_1(V - V_i), \quad (5)$$

$$\frac{dV_i}{dt} = g_1 I_1 - g_2 V_i - g_3 I_1^{1/2} V_i^{3/2}, \quad (6)$$

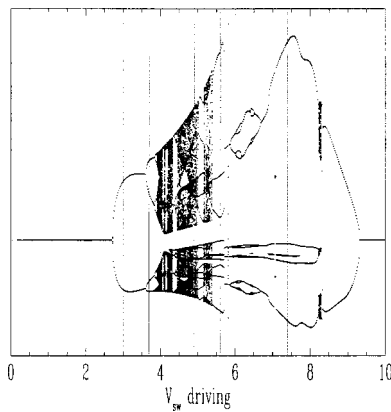


FIG. 1. Bifurcation diagram for the full WINDMI model given in Eqs. (1)–(6). The local maxima and minima found from the cross-tail voltage $V(t)$ are plotted vertically for each fixed V_{sw} value on the horizontal axis. The system goes from a stable fixed point ($V_{sw} < V_1 \approx 2.7$) to a limit cycle ($2.7 < V_{sw} < 3.6$), though a period doubling sequence of bifurcations to chaos, and then through the inverse bifurcations to a state of steady unloading.

where the coupled current loop equations (\dot{I}, \dot{I}_1) have been diagonalized. The ten dimensionless parameters define a parameter vector \mathbf{P} that characterizes the global state of the magnetosphere–ionosphere system. General properties of the four magnetosphere–ionosphere states S1, S2, S3, S4 are discussed in Ref. 3. A system that appears to conform closely to the known wave forms of the classic internally triggered type I substorms is defined by the following parameter values: $\mathbf{P}(S3) = [a_1 = 0.247, a_2 = 0.391, b_1 = 10.8, b_2 = 0.0752, b_3 = 1.06, d_1 = 2200, f_1 = 2.47, g_1 = 1080, g_2 = 4, g_3 = 3.79]$. The dimensionless time scale $\Delta t = 1$ for this state corresponds to 20 min.

The system of Eqs. (1)–(6) provides a mathematical-physics prediction system that takes solar wind input data and yields six major energy components of the magnetosphere–ionosphere system. A recent work¹⁵ pursues the use of the system as a network for the prediction of substorms by optimizing the values of \mathbf{P} over a substorm database. The optimization is carried out by setting the acceptable physical range of each parameter and then using a minimization of the average relative variance of the difference between the prediction and the data. A more direct method for the construction of prediction filters is to use local linear ARMA filters^{16,17} or neural networks.¹⁸ These network methods contain many adjustable weights—typically more than 100 weights. Thus, they will generally produce a lower error in a metric, such as the average relative variance, than the physics models. The nonlinear filters require extensive training on a substorm database to derive the value of the weights. Issues such as the origin of the chaotic behavior from either the solar wind or the internal nonlinear dynamics, however, cannot be resolved by these nonlinear black box methods.

The bifurcation sequence for the S3 state as the solar wind voltage increases from $V_{sw} = 0$ to 10 (≈ 200 kV) is shown in Fig. 1. Briefly described, at $V_{sw} = 2.6$, there is a bifurcation from a stable fixed point (ground state magnetosphere) to a limit cycle. At $V_{sw} \approx 3.6$, a period doubling bi-

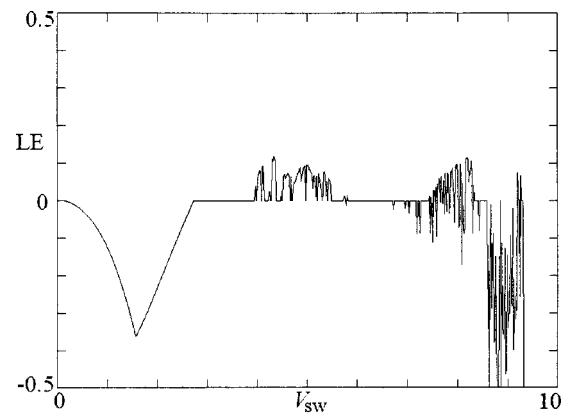


FIG. 2. Largest Lyapunov exponent for the four-dimensional model given in Eqs. (1)–(4), using Eqs. (7) and (8).

furcation sequence begins culminating in chaotic bands. Then for $V_{sw} > 5.5$ a sequence of inverse bifurcations occurs, taking the system to a steady state with high-level convection.

IV. REDUCTION TO A MINIMAL 3-D DYNAMICAL MODEL

A reduced form of Eqs. (1)–(6) results from setting the last two time derivatives [in Eqs. (5) and (6)] to zero and solving for I_1 and V_i , giving

$$V_i = V + a_2(V_{sw} - V)/f_1, \quad (7)$$

$$I_1 = g_3^2 V_i^3 / 2g_1^2 + g_2 V_i / g_1 + (g_3 V_i^2 / 2g_1^2)(4g_1 g_2 + g_3^2 V_i^2)^{1/2}. \quad (8)$$

The full solution relaxes to these fixed points in the (nonlinear) $R_1 C_1$ time scale of $1/[g_2 + g_3(I_1 V_1)^{1/2}]$, which for the S3 state is short, $\approx 10^{-1}$, corresponding to a few minutes. Substituting Eqs. (7) and (8) into Eqs. (1)–(4) yields the first reduced system. [The negative branch of the square root function in Eq. (8) is not physically accessible.]

The reduced four-dimensional system obtained by using Eqs. (7) and (8) to eliminate Eqs. (5) and (6) was solved numerically. The results are very similar to the bifurcation diagram shown in Fig. 1 for the full system, Eqs. (1)–(6), shown in Fig. 1. Figure 2 shows the largest Lyapunov exponent for the reduced system plotted versus V_{sw} .

Negative values of the largest Lyapunov exponents imply stable fixed point solutions, zero values imply limit cycles or perhaps toruses, and positive values imply chaos. The attractors in the various regions resemble those for the full 6-D system. In the chaotic region, the Lyapunov exponent is typically about 0.1, implying a growth time of errors in the initial conditions of about 3 h. The calculation uses a fourth-order Runge–Kutta integrator with a step size of 0.1 and 200 000 iterations for each V_{sw} value.

From numerical experiments, it turns out that a_2 can be set to zero and the ionospheric voltage V_i taken equal to the cross-tail convection voltage $V_i = V(t)$ eliminating Eq. (6) without destroying the chaos, which gives a plot similar to that of Fig. 2. This last reduction eliminates g_1 , g_2 , and g_3

from the dynamics, which is a strong reduction that deserves further investigation in a future work. Furthermore, Eq. (4) can apparently be eliminated as well, giving $K_{\parallel} = P^{1/2}V$, for which chaos still occurs. Finally, the cross-tail voltage V in Eq. (3) can be replaced with its equilibrium value of V_{sw} . Putting in all these simplifications gives the following 3-D system:

$$\frac{dI}{dt} = a_1(V_{sw} - V), \quad (9)$$

$$\frac{dV}{dt} = b_1I - b_2P^{1/2} - b_3V, \quad (10)$$

$$\frac{dP}{dt} = V_{sw}^2 - P^{5/4}V_{sw}^{1/2}\{1 + \tanh[d_1(I-1)]\}/2. \quad (11)$$

A further simplification results from replacing the dimensionless pressure P in Eq. (11) with its equilibrium value, $P = (b_1/b_2 - b_3V_{sw}/b_2)^2$. Now define new variables,

$$x = d_1(I-1), \quad (12)$$

$$y = a_1d_1(V - V_{sw}), \quad (13)$$

$$z = a_1b_2d_1P^{1/2} - a_1d_1(b_1 - b_3V_{sw}), \quad (14)$$

in terms of which the 3-D system above can be written as

$$\frac{dx}{dt} = -y, \quad (15)$$

$$\frac{dy}{dt} = c_1x - b_3y - z, \quad (16)$$

$$\frac{dz}{dt} = -c_2 - c_3 \tanh(x), \quad (17)$$

where

$$c_1 = a_1b_1,$$

$$c_2 = \frac{1}{4}a_1d_1(b_1 - b_3V_{sw})^{3/2}(V_{sw}/b_2)^{1/2} - a_1b_2^2d_1V_{sw}^2/2(b_1 - b_3V_{sw}),$$

and

$$c_3 = \frac{1}{4}a_1d_1(b_1 - b_3V_{sw})^{3/2}(V_{sw}/b_2)^{1/2}.$$

The condition that $b_3V_{sw} < b_1$ is that there be a finite part of the cross-tail current driven by the magnetohydrodynamic (MHD) pressure gradient $j \times B = \nabla p$ condition at the point where I hits the critical current I_c . Here $c_3 > c_2 > 0$, and a_1, b_1, b_3 are positive for the physical regimes.

The system has thus been reduced to one with six terms, four parameters, and a single nonlinearity. To verify that the approximations are reasonable, the largest Lyapunov exponent for this system is plotted versus V_{sw} in Fig. 3(a). Figure 3(b) shows the Lyapunov dimension D_L , and Fig. 3(c) shows the bifurcation diagram for the reduced system. The dimension of the attractor in the chaotic regime is only slightly greater than 2.0 and is consistent with calculations of the correlation dimension (not shown).

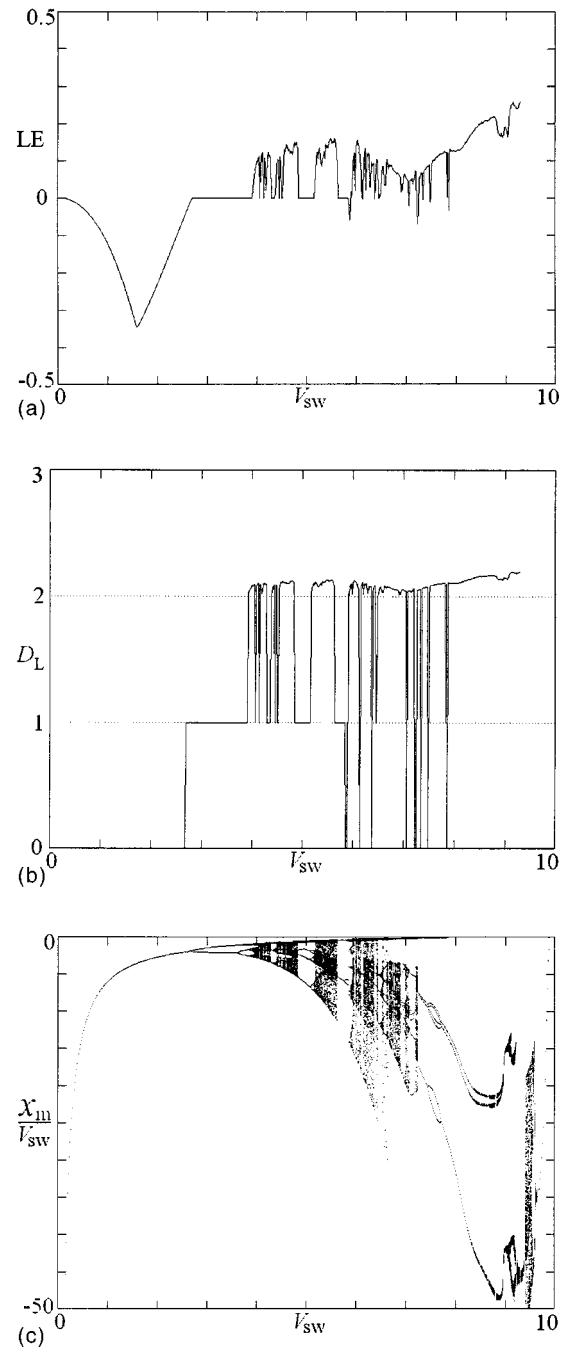


FIG. 3. Dynamical features of the fully reduced three-dimensional system of equations (9)–(11). A comparison with Fig. 2 shows that the transitions between orbit types is well preserved in the minimal model. (a) Largest Lyapunov exponent (LE) as a function of the solar wind dynamo voltage. (b) Lyapunov dimension D_L of the system. (c) Bifurcation diagram constructed from the turning points of $x(t) \propto I(t) - I_c$ as a function of V_{sw} .

There should be little doubt that the hyperbolic tangent is the important nonlinearity in producing the chaos. The 3-D system has a fixed point at $x^* = -\tanh^{-1}(c_2/c_3)$, $y^* = 0$, $z^* = c_1x^*$ with eigenvalues λ that satisfy

$$\lambda^3 + b_3\lambda^2 + c_1\lambda + c_3 - c_2^2/c_3 = 0.$$

A Hopf bifurcation occurs at $c_1b_3 = c_3 - c_2^2/c_3$, followed by a period doubling route to chaos.

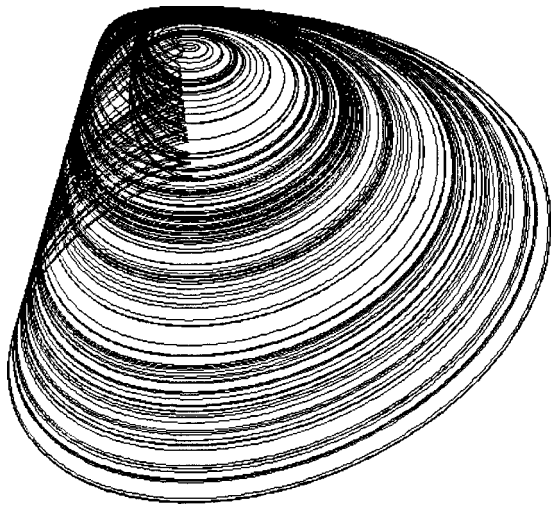


FIG. 4. Relation of current $x(t)$ (vertical) vs voltage $y(t)$ (horizontal), showing the characteristic substorm cycles centered about the critical current $I_c(x=0)$ and the solar wind driving voltage $V_{sw}(y=0)$. In the growth phase the current rises clockwise from the lower left to the upper left, reaching the unloading event at the cusp at the upper left center. Then the rapid expansion phase of the substorm starts, with the trajectory moving clockwise to the right to the maximum cross-tail voltage. Finally, the substorm recovery stage begins, taking the trajectory back to the lower left position to repeat the substorm cycle over with a chaotic relationship between the cycles. The orbits cross because this is a projection of the 3-D phase space (with no crossings) onto the 2-D surface.

For this system, the sum of the Lyapunov exponents is $-b_3$. From the calculated value for the largest exponent and the fact that one exponent must be zero, the entire spectrum can be obtained for the above parameters with $V_{sw}=4.8$ as $(0.145, 0, -1.205)$. The Lyapunov dimension is $2 + 0.145/1.205 = 2.12$, in good agreement with the calculated correlation dimension of 2.14. A phase-space plot of the attractor projected onto the x (vertical)- y (horizontal) plane for these parameters is shown in Fig. 4.

The 3-D system in Eqs. (12)–(14) is equivalent to a jerk form:¹⁹

$$\frac{d^3x}{dt^3} + b_3 \frac{d^2x}{dt^2} + c_1 \frac{dx}{dt} = -c_2 - c_3 \tanh(x), \quad (18)$$

for a third-order explicit ordinary differential system with a scalar variable. This is a special case of a damped harmonic oscillator driven by a nonlinear memory term, whose solutions have been studied and are known to be chaotic. The period of the dominant frequency of oscillation is $2\pi/c_1^{1/2} = 3.85$, corresponding to a real time of about 1 h. In Eq. (18), t can be rescaled by $c_1^{1/2}$ to eliminate one of the four coefficients. The dynamical behavior is thus determined by only three parameters. The regions of various dynamical behaviors are plotted in the $b_3 - V_{sw}$ plane in Fig. 5, with the other parameters, as listed above.

This reduced system (18) could be implemented electronically since a saturating operational amplifier produces a good approximation to the $\tanh(x)$ function, although the behavior is somewhat sensitive to the exact nature of the nonlinearity. A circuit for analog solutions of the 3-D system is shown in Fig. 6. More information on the use of circuits with

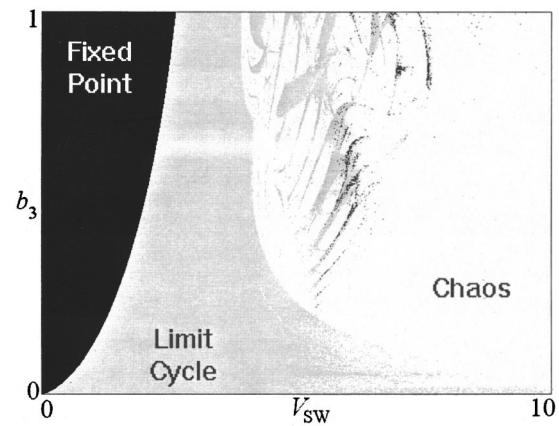


FIG. 5. Characterization of the dynamical behavior of the system as a function of solar wind driving strength (V_{sw}) and ionospheric damping (b_3). The extremely complex (fractal) boundaries between the different types of orbits show the intrinsic limits of predictability of the physical system with imprecise knowledge of the system's parameter vector \mathbf{P} . For a magnetic cloud encounter with the Earth, the solar wind voltage moves slowly across the plane.

operational amplifiers and diodes to represent such physical systems is given in Ref. 20.

V. COMPARISON OF THE FULL AND REDUCED SYSTEMS

The internal deterministic chaos of the two models for the chosen reference parameters appears similar from the chaotic system measures calculated in Sec. III. Here we show how the differences appear in the time series of the independent variables that determine the global energy components. We start the two systems from the same initial values and with the same parameters and show the results in Fig. 7 for the cross-tail lobe current and the cross-tail convection electric field or voltage. The pressure and other variables can be computed readily. We see that the two signals, while similar in shape and having the same number of large (three) and small (five) events, shift phase with respect to one another. In preparing Fig. 7 we make one time shift to bring the first major energy event into phase agreement for the 6-D and 3-D systems. Subsequently, the signals drift into and out of phase with respect to each other. The second major substorm event occurs first in the 6-D model at $t = 37$ and afterward at $t = 38$ in the 3-D model. This shift of $\Delta t = 1$ corresponds to about 20 min for typical magnetosphere–ionosphere parameters. From Fig. 7 this is

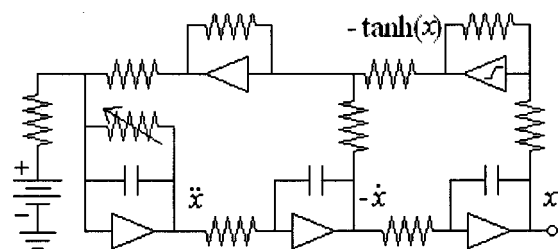


FIG. 6. Analog electric circuit computer that obeys the reduced third ordinary differential equation system for the reduced WINDMI model.

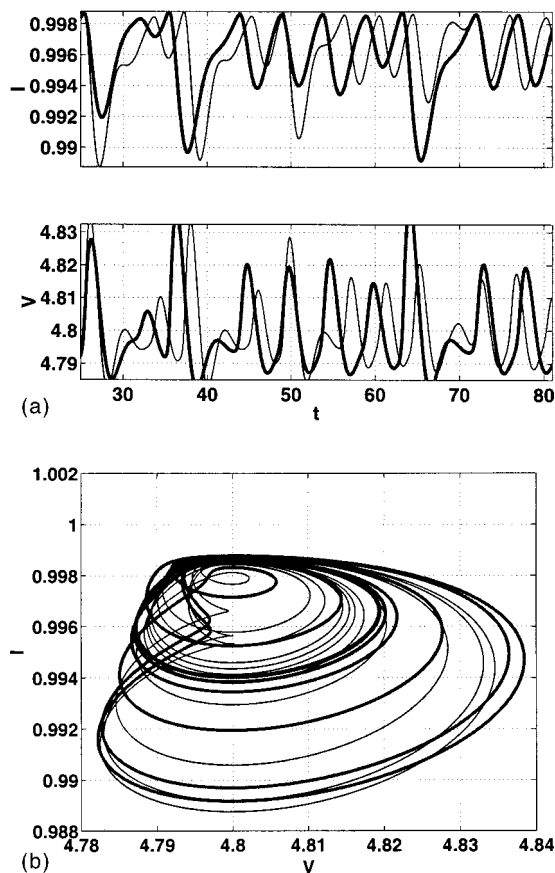


FIG. 7. (a) Time series comparison of a reduced 3-D system with a full 6-D system for state S3. Time series are shifted once in time to a point where (V, I) of the 3-D system has the same value of (V, I) as the 6-D system at the first, large substorm at $t = 10$. The time unit is roughly 20 min for typical M-I parameters. (b) A phase portrait comparison of (V, I) for a reduced 3-D system with a full 6-D system for state S3.

comparable to the full width at half-maximum of the substorm event time. For the full run of $t = 80$ (approximately 27 h) there are three strong events and five moderate strength events. The strengths of the moderate level events are comparable between the two substorm models: the timing of three of the five agree within five minutes or so, while two events have a substantial timing difference. Thus, there is broad agreement between the predictions of the two systems, but the arrival times of the energetic events contains a large uncertainty. This uncertainty in arrival times suggests that we look at the probability distributions of the substorm recurrence times for a long run with many large events.

In Fig. 8 we show the probability distributions of the time between similar energetic events, as calculated from taking a surface of section plot for $x = x_c$. We run the two systems for long times (10^5 dimensionless time steps) and record the time intervals between the crossing of the surface of the threshold set by the surface of section. Figure 8 shows the resulting distributions of these time intervals. The recurrence time distributions are seen to be exponential to a good approximation: the difference in timing shows up here as a difference in the mean time for the substorm recurrence rate. Both models predict a Poisson (or exponential) distribution

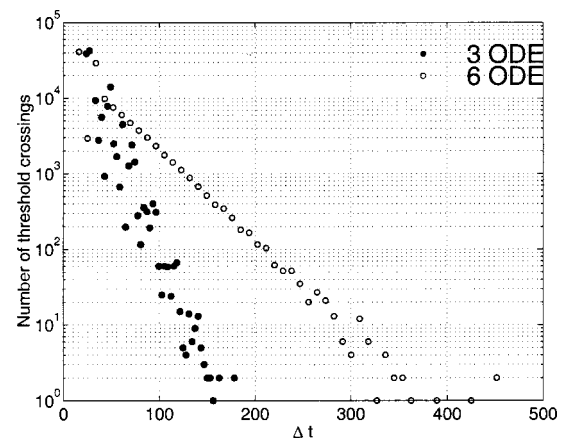


FIG. 8. The time between upper threshold crossings, Δt , at $x_c = I_{\text{cross}}/I_{\text{crit}} = 0.9988$, for a reduced 3-D system and for a 6-D system.

of the recurrence times for the case of constant solar wind driving.

Probability distributions for the convection electric field and the mean plasma pressure at the time of crossing x_c show non-normal distributions. The distributions are skewed toward large events with an exponential-like decay rather than a Gaussian decay for large events. Thus, the models predict an excess of large substorm events over that which would be obtained for adding Gaussian noise to the system. This is one signature of the internal storage and release mechanism contained in these models used to describe the substorm dynamics. Large MHD simulations with constant solar input drivings also show the storage and release mechanism operating in the solar-wind-driven magnetosphere.

VI. CONCLUSIONS AND DISCUSSION

Starting from the six-dimensional nightside magnetosphere–ionosphere WINDMI model with ten dimensionless physics parameters, we eliminate the fast-evolving fields to derive a new minimal 3-D model of the wind-driven magnetosphere–ionosphere system. Comparisons of the bifurcation properties and the nature of the attractors shows the preservation of the essential features of the full model. Both models make a complex transition from stable fixed points to chaos and back to a high-level fixed point, with the complex boundary shown in detail with a two-parameter subspace shown in Fig. 5. In the chaotic regime of parameter space there is an intrinsic limit to the prediction time, found to be in the range of 3–5 h for the wind-driven Earth magnetosphere–ionosphere system. Viewed as a space weather problem, other effects that limit the predictability of the system arise from uncertainties in initial data, possible errors in the physical parameters, and the external stochasticity of the solar wind.

Including the external stochasticity does not change the character until a threshold is reached, where the excursions induced in the cross-tail convection field become comparable to the oscillations of the field from the substorm cycles.² When the external stochastic driver is dominant then the statistics of the magnetosphere–ionosphere fields will be essentially the same as those for the external drive. Thus, for nor-

mally distributed solar wind fluctuations, we would expect to see quasinormal output distributions with small kurtosis and skewness in the internal magnetosphere–ionosphere variables. These statements need to be modified, of course, when the internal system is near the critical point for unloading or when there is a sufficiently fast drop in the solar wind driving voltage. In these cases the external driver can act as the triggering agent for the substorm event, Refs. 21, 15.

Thus, this analysis of the internal deterministic chaos and modeling with WINDMI makes clear the importance of assembling large substorm databases with a large range of event sizes. Such a new substorm database would also be useful for comparing the predictions from self-organized criticality models, as recently reported by Uritsky *et al.*,²² using two-dimensional-driven resistive MHD equations with an internal trigger for plasma unloading—not unlike the one used in the WINDMI model.

ACKNOWLEDGMENTS

This work was sponsored by National Science Foundation Grant No. ATM 990763 and by the U.S. Department of Energy Contract No. DE-FG03-96ER-54346.

¹A. M. Fraser and H. L. Swinney, Phys. Rev. A **33**, 1134 (1986); A. M. Fraser, Physica D **34**, 391 (1989).

²B. Goode, I. Doxas, J. R. Cary, and W. Horton, “Differentiating between colored random noise and deterministic chaos,” to appear in J. Geophys. Res.

³J. P. Smith, J.-L. Thiffeault, and W. Horton, J. Geophys. Res. **105**, 12 983 (2000).

- ⁴A. J. Klimas, D. Vassiliadis, D. N. Baker, and D. A. Roberts, J. Geophys. Res. **101**, 13 089 (1996).
- ⁵D. N. Baker, T. I. Pulkkinen, J. Büchner, and A. J. Klimas, J. Geophys. Res. **104**, 14 601 (1999).
- ⁶D. Vassiliadis, A. S. Sharma, T. E. Eastman, and K. Papadopoulos, Geophys. Res. Lett. **17**, 1841 (1990).
- ⁷W. Horton and I. Doxas, J. Geophys. Res. **101A**, 27 223 (1996).
- ⁸W. Horton and I. Doxas, J. Geophys. Res. **103A**, 4561 (1998).
- ⁹J. P. Smith and W. Horton, J. Geophys. Res. **103A**, 14 917 (1998).
- ¹⁰A. Wolf, J. B. Swift, H. L. Swinney, and J. A. Vastano, Physica D **16**, 285 (1985).
- ¹¹J. Kaplan and J. Yorke, “Lecture Notes in Mathematics 730,” in *Functional Differential Equations and the Approximation of Fixed Points* (Spring-Verlag, Berlin, 1979), p. 204.
- ¹²W. Horton, J. Smith, R. Weigel, B. Goode, I. Doxas, and J. R. Cary, Phys. Plasmas **6**, 4178 (1999).
- ¹³W. Horton, M. Pekker, and I. Doxas, Geophys. Res. Lett. **25**, 4083 (1998).
- ¹⁴C. J. Farrugia, M. P. Freeman, L. F. Burlaga, R. P. Lepping, and K. Takahashi, J. Geophys. Res. **98**, 7657 (1993).
- ¹⁵R. S. Weigel, W. Horton, and I. Doxas, WINDMI optimization and performance validation, IFSR#899, <http://orion.ph.utexas.edu/~windmi>
- ¹⁶D. Vassiliadis, A. J. Klimas, D. N. Baker, and D. A. Roberts, J. Geophys. Res. **100**, 3495 (1995).
- ¹⁷D. Vassiliadis, A. J. Klimas, D. N. Baker, and D. A. Roberts, J. Geophys. Res. **101**, 19 779 (1996).
- ¹⁸R. S. Weigel, W. Horton, T. Tajima, and T. Detman, Geophys. Res. Lett. **26**, 1353 (1999).
- ¹⁹J. C. Sprott, Phys. Lett. A **266**, 19 (2000).
- ²⁰J. C. Sprott, Am. J. Phys. **68**, 758 (2000).
- ²¹L. R. Lyons, J. Geophys. Res. **100**, 19 069 (1995).
- ²²V. M. Uritsky, A. J. Klimas, and D. Vassiliadis, “On a new approach to detection of stable critical dynamics of the magnetosphere,” in *Proceedings of the 5th International Conference on Substorms*, St. Petersburg, Russia, ESA SP-443 (European Space Agency, Paris, 2000).